Evolution of complex I–like respiratory complexes

Hongjun Yu[1,*], Gerrit J. Schut[2], Domink K. Haja[2], Michael W. W. Adams[2,*], and Huilin Li[3,*]

From the [1]Department of Biochemistry and Molecular Biology, School of Basic Medicine and Tongji Medical College, Huazhong University of Science and Technology, Wuhan, China; [2]Department of Biochemistry and Molecular Biology, University of Georgia, Athens, Georgia, USA; [3]Department of Structural Biology, Van Andel Institute, Grand Rapids, Michigan, USA

Edited by Ruma Banerjee

The modern-day respiratory complex I shares a common ancestor with the membrane-bound hydrogenase (MBH) and membrane-bound sulfane sulfur reductase (MBS). MBH and MBS use protons and sulfur as their respective electron sinks, which helped to conserve energy during early life in the Proterozoic era when the Earth's atmosphere was low in oxygen. MBH and MBS likely evolved from an integration of an ancestral, membrane-embedded, *m*ultiple *r*esistance and *p*H antiporter and a soluble redox-active module encompassing a [NiFe] hydrogenase. In this review, we discuss how the structures of MBH, MBS, *m*ultiple *r*esistance and *p*H, photosynthetic NADH dehydrogenase-like complex type-1, and complex I, which have been determined recently, thanks to the advent of high-resolution cryo-EM, have significantly improved our understanding of the catalytic reaction mechanisms and the evolutionary relationships of the respiratory complexes.

Respiratory complexes couple the energy from redox reactions to the generation of electrochemical gradients and play a central role in cellular energy generation. Respiratory complex I is the first and most complicated enzyme in the electron transport chain of modern aerobic organisms. It catalyzes electron transfer from NADH to quinone and concomitantly drives protons across the membrane that are subsequently used to conserve energy by ATP synthesis (1–4). Complex I contains a 14-subunit core for redox catalysis and proton translocation. That core is highly conserved from bacteria to higher eukaryotes, although mammalian complex I contains an extra 31 supernumerary subunits (1, 2, 5–8). Mechanistic insights into the function and intricacies of complex I have been gained through structural research, beginning with crystallographic studies of bacteria and yeast complex I, and recently from cryo-EM studies of the mammalian version and supercomplexes containing complex I as a component (9–19).

In oxygenic photosynthetic microorganisms, there are two types of electron transport. One is a linear electron flow, in which electrons extracted from water by photosystem II are passed through cytochrome b_6f and plastoquinone (PQ), reducing NADP$^+$ to NADPH in photosystem I and thereby establishing a proton gradient for ATP synthesis. The second

is a cyclic flow in which electrons are cycled between cytochrome b_6f and photosystem I via PQ. These organisms also contain an NADH dehydrogenase-like complex type-1 (NDH) that functions in cyclic electron flow by transferring electrons from ferredoxin (Fd) to PQ in order to pump protons across a thylakoid membrane, enabling ATP synthesis without concomitant production of NADPH (20, 21). NDH is closely related to complex I; it contains 11 of its 14 core subunits as well as several oxygenic- and photosynthesis-specific subunits. Three cryo-EM structures of the 18-subunit NDH complex isolated from the thermophilic cyanobacterium *Thermosynechococcus elongatus* have been determined recently from samples prepared at various pH values, revealing the overall organization and the Fd and PQ binding modes (22–24).

Energy conservation by complex I–related respiratory systems in some anaerobic microbes within the Archaea shows great variation and complexity; some even utilize Na$^+$ rather than H$^+$ as the coupling ion to drive ATP synthesis (25–28). *Pyrococcus furiosus* is a hyperthermophilic, anaerobic archaeon that resides in hot marine sediments and grows optimally at 100 °C, representing an ancestral life form with great potential in biotechnological applications (29, 30). In *P. furiosus*, two Na$^+$-dependent energy-conserving complexes have been characterized: a membrane-bound [NiFe] hydrogenase (MBH) complex and a membrane-bound sulfane sulfur reductase complex (MBS) (3, 25, 31, 32). MBH functions when the organism grows without elemental sulfur (S°). It falls into group 4 [NiFe] hydrogenases; this is the only group that contains nonhydrogenases, including several other Na$^+$-dependent energy-coupling complexes in related *Thermococcus* species such as carbon monoxide dehydrogenase and formate hydrogen lyase (25, 28, 33). Those complexes transfer electrons from various donors (Fd for MBH; carbon monoxide for carbon monoxide dehydrogenase; and formate for formate hydrogen lyase) to protons and evolve H$_2$ gas. The electron transfer is coupled to the translocation of Na$^+$ across the membrane for subsequent ATP synthesis through the Na$^+$-dependent ATP synthase (26, 34).

However, when *P. furiosus* grows on S°, MBH is downregulated, whereas MBS is upregulated and is essential (31, 35, 36). MBS catalyzes the transfer of electrons from Fd to polysulfide and generates a Na$^+$ gradient, conserving more energy (42 kJ/mol/2e$^-$) than MBH (12 kJ/mol/2e$^-$), with a maximal growth yield coefficient almost twice that obtained without S°

* For correspondence: Huilin Li, Huilin.Li@vai.org; Hongjun Yu, hongjun_yu@hust.edu.cn; Michael W. W. Adams, adamsm@uga.edu.

(3, 37). MBS lacks a molybdopterin cofactor, and it therefore reduces sulfur by a mechanism distinct from the molybdopterin-containing sulfur reductases found in mesophilic bacteria (38, 39). The recent cryo-EM structure of MBS reveals its architecture and provides insights into its catalytic mechanism; together with the recent MBH structure, it sheds lights into their close evolutionary relationship with complex I (40, 41).

One of the most convincing evolutionary relations is the similarity between the [NiFe] hydrogenase catalytic subunits from group 4 and the Q module of complex I, as shown using phylogenetic analysis (3, 42). These homologous modules are illustrated in Figure 1. A rather simple evolutionary pathway has been proposed in which complex I evolved from ancestral [NiFe] hydrogenases and *m*ultiple *r*esistance and *p*H (Mrp) complexes (43), driven by changes in geochemistry and bioenergetics (3). In addition to complex I, MBH, and MBS, several other related complexes have been identified based on genome sequence (3). However, our understanding of the evolution of respiratory complexes has been complicated by the available structures of complex I, MBH, and MBS, which reveal different arrangements of the homologous modules between these complexes.

NDH, MBH, and MBS belong to the complex I–like superfamily of membrane-bound respiratory complexes (44). All the members of this family are believed to have evolved from a common Mrp Na^+/H^+ antiporter complex (41, 43, 45), the structure of which was recently reported (46, 47).

In spite of the great progress described previously, detailed molecular mechanisms for this complex I–like superfamily are still lacking, such as the ion translocating path, utilization of different substrates, coupling of redox reactions to proton translocation, and evolutionary relationship among these complexes. This review focuses on the differences and connections among complex I–like respiratory complexes. We describe how mechanistically relevant modules are differently organized, as well as the unique adaptions of the individual respiratory machineries for various energy needs.

Distinct assembly of shared modules of respiratory complexes

At first glance, all complex I–like respiratory complexes appear similar, with an L-shaped structure consisting of a peripheral arm and a membrane arm (Fig. 1). However, careful structural analyses have revealed that these complexes are assembled differently from a common set of highly conserved functional modules.

Complex I has the longest peripheral arm among these complexes, containing an N module and a Q module (Fig. 1A). The N module is distal to the membrane arm and contains the NADH dehydrogenase activity that extracts low-potential high-energy electrons from NADH (48). It is connected to the membrane proton pumps by the Q module, which is directly attached to the membrane arm *via* a membrane anchor (mammalian ND1; *Thermus thermophilus* Nqo8). The Q module contains four hydrophilic subunits that coordinate

three [4Fe–4S] clusters that relay electrons from the N module to ubiquinone (48). The membrane arm of complex I translocates protons with a stoichiometry of $4H^+$ to $2e^-$, necessitating four proton-pumping units (49–51). It is generally agreed that three large membrane subunits—in mammals: ND2, ND4, and ND5; in *T. thermophilus*: Nqo12, 13, and 14; also called antiporter-like subunits—each form a proton translocation path called the P module in Figure 1A (9–11).

The identity of the fourth proton path is less certain. It may be composed of several smaller membrane subunits (mammalian, ND6, ND4L; *T. thermophilus*, Nqo10, 11) termed the Pc module here (for composite proton path) (10, 11, 52, 53). Alternatively, it may be two half channels, with one half channel in the *T. thermophilus* Nqo8 (mammalian, ND1; the membrane anchor of Q module) and the other half channel in the Pc module (9). The 11 core subunits of NDH (Fig. 1B) are arranged essentially the same as in complex I (22–24). However, NDH has a shorter peripheral arm because of the lack of the three subunits found in complex I that oxidize NADH. Accordingly, NDH transfers electrons from Fd (rather than from NADH) to PQ.

Both MBH and MBS establish a Na^+ gradient across the membrane with redox energy (low-potential high-energy electrons) from Fd. However, MBH transfers electrons to protons rather than to quinone and thus evolves H_2 gas, whereas MBS transfers electrons to reduce the S–S bond of sulfane sulfur (25, 31). Both MBH and MBS are L-shaped structures with a peripheral arm and a membrane arm (Fig. 1, C and D) (40, 41). Interestingly, MBS has evolved specific structural elements that assemble a dimeric complex. These elements include multiple salt bridges and a tryptophan-rich C-terminal extension of one MbsD subunit that extends into a large hydrophobic cleft in the peripheral arm of the second subunit. Each monomeric complex is expected to be fully functional. The peripheral arms of MBH and MBS contain four hydrophilic subunits: MbhJKLN in MBH and MbsJKLN in MBS, and they are closely related to the Q module of complex I. These cytoplasmic subunits are attached to their respective membrane arms through a membrane-anchoring subunit, MbhM in MBH and MbsM in MBS, which are homologous to the membrane-anchoring subunit Nqo8 in complex I. The four hydrophilic subunits together with the membrane anchor form a membrane-anchored peripheral module, a prominent feature conserved among MBH, MBS, NDH, and complex I (Fig. 1).

Despite the high degree of structural conservation, major architectural and mechanistic differences exist among the respiratory complexes. First, the membrane-anchored peripheral module is attached to the "left" side of the membrane module of complex I and NDH (Fig. 1, A and B) but is attached to the "right" side of the membrane module of MBH and MBS (Fig. 1, C and D). This architectural difference may suggest different proton translocation mechanisms, which are described later. Second, while neither complex I nor NDH translocate Na^+, MBH and MBS each contains a Na^+-translocating module that is homologous to the Na^+-translocating module found in the Mrp antiporter (46, 47). In fact, Mrp has
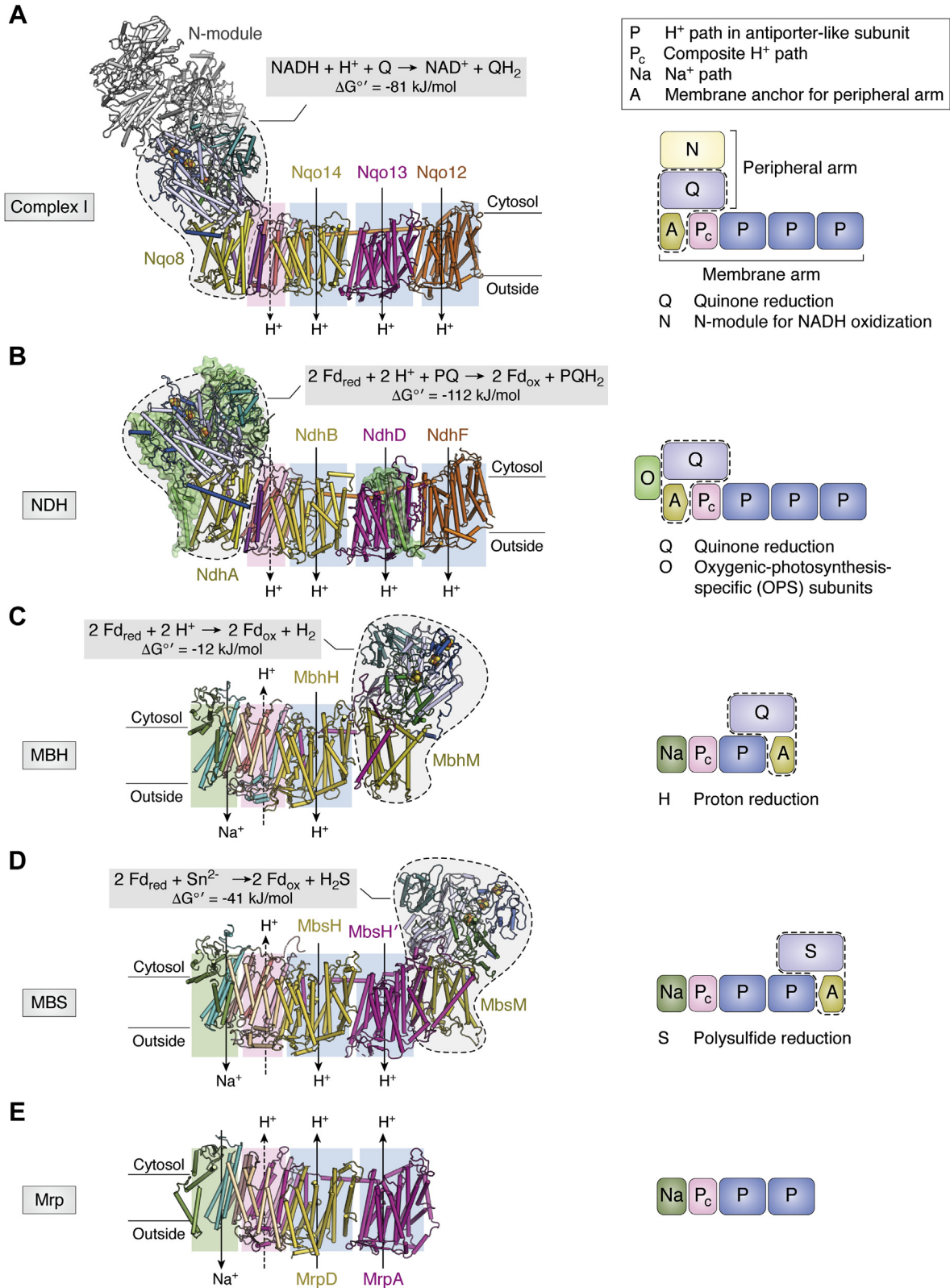
Figure 1. Modular architecture of complex I–like respiratory complexes. *A–E*, the structures and proposed working models of complex I–like family members: (*A*) complex I (*Thermus thermophiles*; Protein Data Bank [PDB] ID: 4HEA); (*B*) NDH (PDB ID: 6HUM) with OPS subunits highlighted in *transparent green* surface view; (*C*) MBH (PDB ID: 6CFW); (*D*) MBS (PDB ID: 6U8Y); and (*E*) Mrp (PDB ID: 6Z16). The outlined region is the membrane-anchored peripheral module conserved among these complexes. The *colored* and *shaded boxes* in the *left panel* mark the modules corresponding to the schematic representation in the *right panel*. MBH, membrane-bound hydrogenase; Mrp, *m*ultiple *r*esistance and *p*H; NDH, NADH dehydrogenase-like complex type-1; OPS, oxygenic photosynthesis-specific.

every ion-translocating unit found in MBS (Fig. 1*E*). However, the number of H$^+$-translocating units varies in these complexes: MBH has two, MBS and Mrp each have three, and NDH and complex I each have four (Fig. 1, *A*, *C* and *D*). Nevertheless, in each complex, one H$^+$-translocating unit is universally made of the composite Pc path.

Proton and sodium translocation

Here, we present a detailed structural comparison to identify features important for proton and sodium translocation, in an attempt to understand how MBH, MBS, and Mrp have maintained the Na$^+$/H$^+$ antiporter activity and how NDH and

complex I may have evolved to only pump protons by abolishing the Na$^+$ translocation capability (1, 41–43, 45).

H$^+$ translocation is the most conserved feature among these respiratory complexes. There are two types of proton paths in each complex. Type I is contained within antiporter-like subunits, whereas type II is the composite Pc path (Fig. 2). Type I proton paths are the most conserved and best understood (9–11). MBH has one (MbhH) and MBS has two (MbsH and MbsH′), whereas NDH and complex I each have three (9–13, 15, 16) (Fig. 2*A*). Key elements associated with proton translocation include two half channels in each transporter-like subunit, a transmembrane helix break in each half channel (in MbsH, TMH7 and 12; in MbsH′, TMH7 and 12), and a
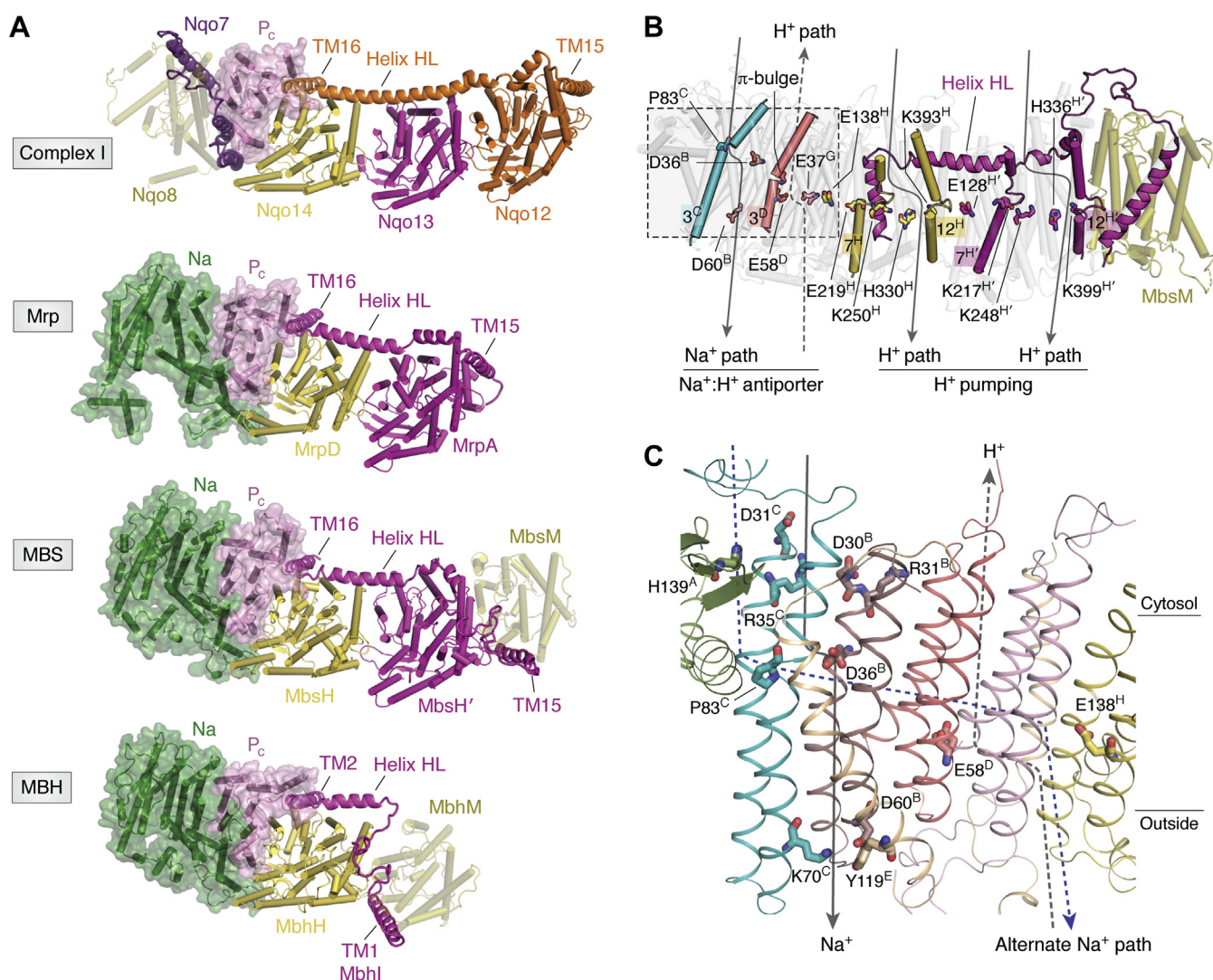
Figure 2. Ion translocation mechanism in membrane arms of complex I–like complexes. *A*, comparison of membrane arms of complex I, Mrp, MBS, and MBH (the sources of the structures are the same as in Fig. 1). Structural alignment was based on their respective antiporter-like subunit: Nqo14 of complex I, MrpD of Mrp, MbsH of MBS, and MbhH of MBH. The aligned structures are shown separately for clarity. Antiporter-like subunits are illustrated as *cartoons*; membrane anchor in the peripheral arm as *semitransparent cartoons*; and Na module and Pc module as *green* and *pink* surfaces, respectively. *B*, proposed ion translocation paths across each module (P module; Pc module; and Na module) are illustrated on the membrane arm of MBS. A prominent central hydrophilic axis (with the residues labeled) extending across the membrane arm is formed. For the Na$^+$ translocation activity of MBS, the Na$^+$ path and H$^+$ path together may form a putative Na$^+$:H$^+$ antiporter module for the exchange of Na$^+$ and H$^+$. *C*, zoom view of the putative Na$^+$ translocation path as marked by the *dashed box* in (*B*). The superscript letters on the amino acid labels refer to subunit identities. The Na$^+$ path is illustrated as a *solid gray arrow*, and the H$^+$ path is illustrated as a *dashed gray arrow*. This is based on the MBS structure (40). An alternative Na$^+$ path involving similar key residues (*dashed blue arrow*) was put forth based on the Mrp structure (46). MBH, membrane-bound hydrogenase; MBS, membrane-bound sulfane sulfur reductase; Mrp, *m*ultiple *r*esistance and *Ph*.

charged axis extending across membrane interior (in MbsH, E138, E219, K250, H330, and K393; in MbsH′, E128, K217, K248, H336, and K399) (Fig. 2*B*). These features are highly conserved among antiporter-like subunits of complex I–like machineries and suggest there is only one proton path within each antiporter-like subunit; this suggestion is supported by mutagenesis studies and molecular dynamics simulations (9–11, 22, 23, 40, 41, 46, 54–56).

Notably, a lateral helix (helix HL) is universally conserved; it integrates all type I antiporter-like proton paths in each respiratory complex (Fig. 2*A*). Helix HL is the longest in complex I, as it connects together three antiporter-like subunits. Helix HL is shorter in MBH, MBS, and Mrp, just long enough to span one (in MBH) or two (in MBS and Mrp) type I proton paths. The sizes suggest an important role of the lateral helix in maintaining the assembly of varied numbers of antiporter-like subunits in complex I–like machineries (57, 58).

The type II Pc proton paths are putative because their precise mechanism is not well understood (9, 10, 52). The Pc paths are half the size of type I paths and composed of multiple subunits. Pc paths resemble type I paths in terms of charged resides and a helical distortion. For example, the Pc path in MBS, composed of MbsD, MbsG, and TMH1-2 of MbsE, contains the conserved charged residues E58 in MbsD and E37 in MbsG, and a π-bulge distortion in TMH3 of MbsD (3^D; Fig. 2*B*). These features are also present in complex I and MBH (10, 11, 14, 17, 18, 41, 52).

Located adjacent to the type II Pc proton path in MBH, MBS, and Mrp is another multiple-subunit module with Na^+ translocation activity (Fig. 2, *A* and *B*). This composite Na^+ path is absent in complex I, which does not translocate Na^+. The deletion of this module diminished Na^+-dependent H_2 production in MBH (41). The MBH, MBS, and Mrp structures have several conserved features essential for Na^+ translocation (40, 41), and we will use the MBS structure as an example. At the cytoplasmic side are four conserved charged residues (in MbsB, D30 and R31; in MbsC, D31 and R35) that may serve as the entry sites for Na^+ (Fig. 2*C*). Replacement of the MbsB D30 and R31 equivalents in Mrp by alanine abolished or reduced its H^+/Na^+ antiporter activity (59). There are two conserved negatively charged cavities below the Na^+ entry site that form a complete Na^+ translocating path (Fig. 2*C*). The first cavity reaches halfway through the membrane and is close to the absolutely conserved MbsB D36. Replacing a leucine for the equivalent aspartate residue in Mrp abolished antiporter activity (46).

Adjacent to the first negatively charged cavity is the conserved P83 in MbsC that breaks TMH3 into two half helices; this is a prominent feature found in other H^+/Na^+ antiporters (60–63). The second cavity is close to the outside of the membrane, involving D60 of MbsB (conserved) and K70 of MbsC and Y119 of MbsE (conserved only as polar residues). It is less negatively charged, perhaps to facilitate the release of Na^+ outside the membrane. An alternative Na+ translocation path was suggested based on the cryo-EM structure of *Anoxybacillus flavithermus* Mrp (Fig. 2*C*) (46). It has a similar Na^+ entry site involving the conserved MbsB D30 and MbsA H139

and a similar first negatively charged cavity containing MbsB D36; but it has a different Na^+ outlet, which coincides with the proton entry pathway in the proposed Pc unit of MBH and MBS (40, 41). Yet another cryo-EM structure of the *Dietzia* Mrp suggested that the antiporter-like subunit MrpD may translocate Na^+ (47), which is different from both models described previously. Therefore, the current Na^+ translocation paths in the MBH and MBS respiratory complexes are speculative and require further investigation.

The four-proton translocation stoichiometry of complex I is generally accepted and enjoys strong experimental support, although its fourth type II proton path (the Pc path) is less defined (Fig. 1*A*). However, the proton translocation mechanisms of MBH and MBS are primarily based on structures and therefore are much less well defined (Figs. 1 and 2*B*). Here, we distinguish type II Pc path into two categories: first, the Pc path in complex I or NDH, which is highly constrained (sandwiched between the membrane-anchoring subunit to the left and the HL-integrated type I proton path to the right), and second, the Pc path in MBH, MBS, or Mrp, which is less constrained because the membrane-anchoring subunit is either absent (in Mrp) or moved away to the far right side (in MBH and MBS) (Figs. 1 and 2*A*). We hypothesize that tight constraint in complex I and NDH forces the Pc unit to actively translocate protons in unison—in the same direction—with the three type I proton paths. Without the constraint of the membrane-anchoring unit, the type II Pc unit in Mrp, MBH, or MBS pairs with the Na^+-translocating unit to function as a passive Na^+/H^+ exchanger (Fig. 1, *C* and *D*) (40, 41). Our hypothesis provides a rationale for the opposing locations ("left" *versus* "right") of the membrane-anchored peripheral redox modules among the MBH, MBS, NDH, and complex I respiratory complexes. The scheme of separating type II Pc units into active proton pumps and passive Na^+/H^+ exchangers is consistent with the energy conservation efficiency of these complexes (calculated under standard conditions): 81 kJ/mol/2e^- for complex I with four proton pumps, 41 kJ/mol/2e^- for MBS with two proton pumps, and 12 kJ/mol/2e^- for MBH with only a single proton pump (3).

Comparison of the redox reaction site

As described previously, the peripheral arm and its membrane anchor constitute the membrane-anchored peripheral module that is conserved among complex I, NDH, MBS, and MBH (Fig. 1) (40, 41). The proximal half (for MBS, MbsL and MbsJ; MBH, MbhL and MbhJ; and *T. thermophilus* complex I, Nqo4 and Nqo6) directly contacts the membrane anchor (for MBS, MbsM; MBH, MbhM; and *T. thermophilus* complex I, Nqo8), and there is a large chamber at the interface that is of similar size in all these complexes (Fig. 3*A*). However, the entrance to the chamber is more open in MBS and complex I than in MBH (40). This is consistent with the need to allow access to hydrophobic polysulfide and ubiquinone in MBS and complex I, respectively.

The conserved peripheral arm coordinates a chain of three [4Fe–4S] clusters in all these complexes where the distances
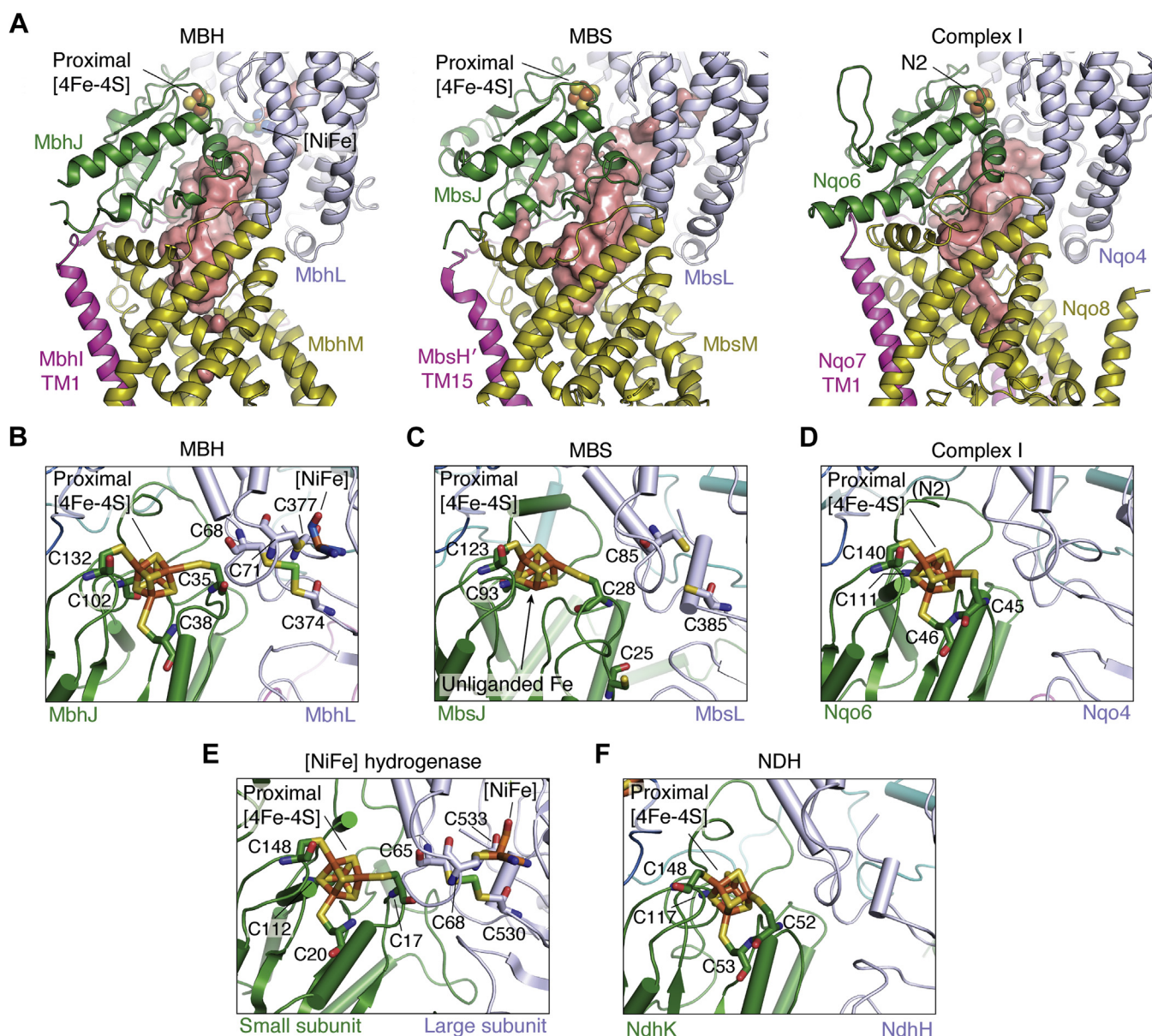
Figure 3. Redox active sites in complex I–like respiratory complexes. *A*, the peripheral module is conserved among MBH, MBS, and complex I. A chamber of similar size is formed between the peripheral arm and its membrane anchor (MBH, MbhM; MBS, MbsM; complex I, Nqo8) in all three complexes and is shown in salmon surface. Structural alignment is based on the MBH MbhL, MBS MbsL, and complex I Nqo4; the aligned structures are shown separately for clarity. The sources of structures are the same as in Figure 1. *B–F*, comparison of the mode of coordination of proximal [4Fe–4S] cluster in complex I–like complexes. The complexes are aligned by MbhL in MBH (Protein Data Bank [PDB] ID: 6CFW), MbsL in MBS (PDB ID: 6U8Y), Nqo4 in complex I (PDB ID: 4HEA), the large subunit of [NiFe] hydrogenase (PDB ID: 2FRV), and NdhH in NDH (PDB ID: 6HUM). The aligned structures are shown separately for clarity. MBH, membrane-bound hydrogenase; MBS, membrane-bound sulfane sulfur reductase; NDH, NADH dehydrogenase-like complex type-1.

between cluster edges are less than 12 Å, enabling efficient electron tunneling (64). The distal and medial [4Fe–4S] clusters are each coordinated by four cysteines: MbsN C61, C64, C67, and C106 for the distal and C71, C96, C99, and C102 for the medial cluster in MBS. This is similar among MBS, MBH, NDH, and complex I (40, 41).

The proximal [4Fe–4S] clusters are the top of the substrate-binding chambers, and they are differently coordinated, consistent with their distinct redox substrates, that is, ubiquinone for complex I, protons for MBH, and polysulfide for MBS (Fig. 3, *B–F*). In MBH, four cysteines in MbhJ coordinate the proximal [4Fe–4S] cluster, holding it within the electron-

tunneling distance of the [NiFe] cluster, which is site of H_2 catalysis and also coordinated by four cysteines in MbhL. This mode of coordination resembles that of soluble dimeric [NiFe] hydrogenase and enables electron flow from the proximal [4Fe–4S] cluster to the [NiFe] cluster for proton reduction (Fig. 3, *B* and *C*) (41). In complex I and NDH, the proximal [4Fe–4S] clusters (also called N2) are also coordinated by four cysteines. However, two of the four cysteines are consecutive in the primary sequence: Nqo6 C45 and C46 in complex I and NdhK C52 and C53 in NDH. They form a unique coordination geometry that allows for direct protonation and electron transfer to ubiquinone or PQ, respectively, although the exact

mechanism is still unknown (Fig. 3, *D* and *E*) (48). In MBS, however, the proximal [4Fe–4S] is coordinated by three, not four, cysteines (Fig. 3*F*). Therefore, one of the four Fe ions is unliganded and has been proposed to function as the catalytic center for reducing inorganic polysulfide (40). This sulfur respiration mechanism is novel, distinct from the known sulfur reduction mechanism in mesophilic bacteria involving a molybdopterin (38, 39).

Compared with MBH, complex I and NDH have lost all four cysteines coordinating the [NiFe] cluster and do not have hydrogenase activity (Fig. 3, *B–E*). In MBS, however, there is a vestige of the [NiFe] binding site: of the four cysteines coordinating the [NiFe] in MBH, two remain in MBS (C85 and C385), although they can no longer coordinate a [NiFe] cluster (Fig. 3*F*). Surprisingly, they are not involved in catalysis even though they are conserved (40). Therefore, the structures suggest a gradual evolution of the [NiFe] site from a soluble [NiFe] hydrogenase, to MBH, then to MBS, and finally to NDH

and complex I (44, 65). While the active site among these complexes and the associated substrates are vastly different, the structure around the three [4Fe–4S] clusters is highly conserved, including the three-loop structure as depicted in Figures 3 and 4. It is likely that this chain of three clusters is more important for energy transduction than the substrate active site, and it may explain the evolutionary success of these respiratory complexes.

Energy conversion by physical coupling of redox reaction with proton translocation

The exact mechanism for coupling electron transfer to the spatially separated proton translocation remains unresolved (1, 2, 6–8, 40, 41). A dynamic region at the interface between the peripheral arm and membrane arm is proposed to be important for the energy transduction in complex I (9–11, 14). Specifically, quinone reduction
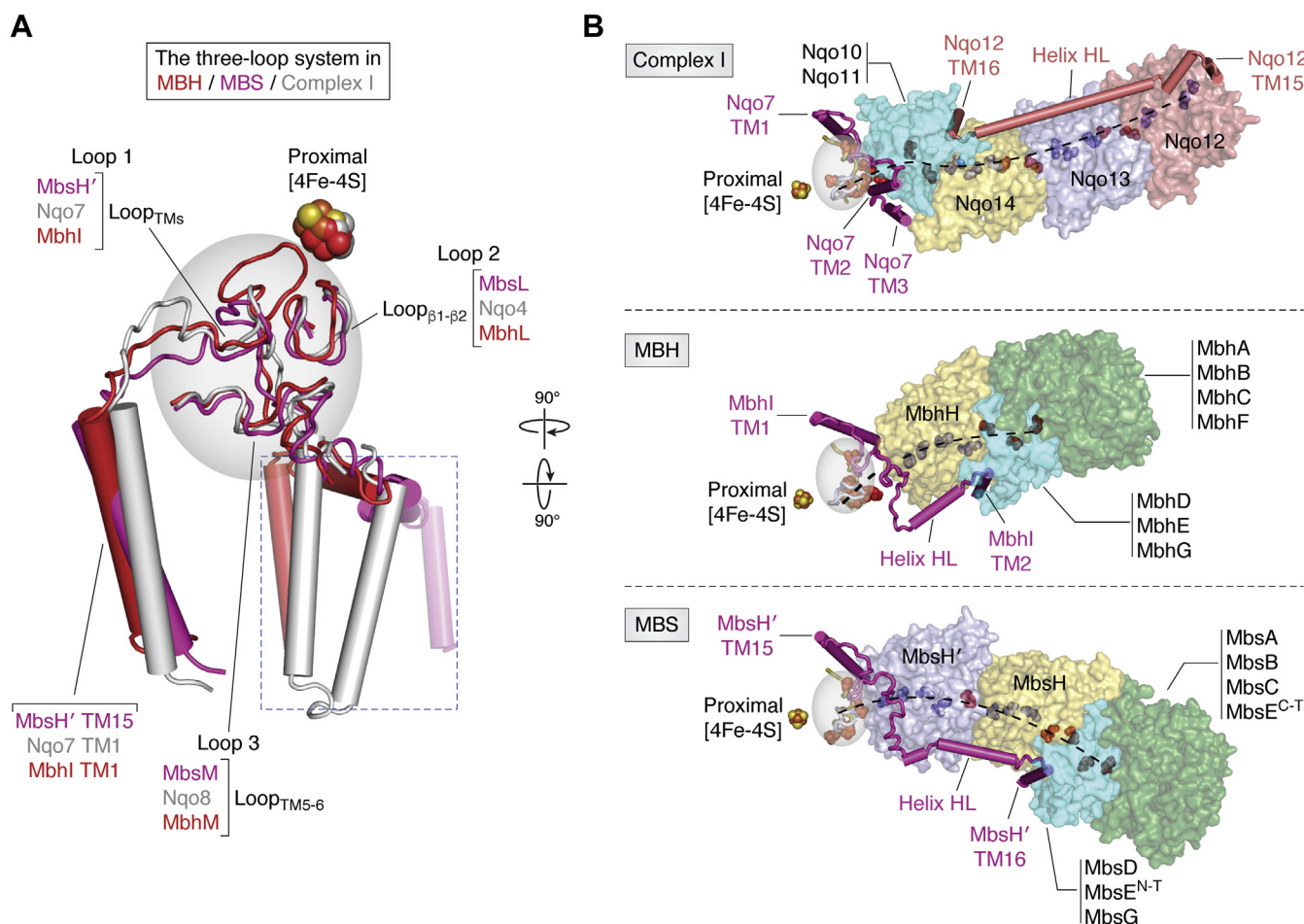
Figure 4. Conserved structural elements for energy conversion in complex I–like respiratory complexes. *A*, the three interfacial loops (in the *shaded area*) are in a comparable configuration in respiratory complex MBH (in *red*), MBS (in *magenta*), and complex I (in *gray*). The three loops are loop$_{two-TMs}$ (loop 1), loop$_{\beta1-\beta2}$ (loop 2), and loop$_{TM5-6}$ (loop 3). They are adjacent to the proximal [4Fe–4S] cluster, at the interface between the peripheral arm and its membrane anchor in each complex. The structural conservation is revealed by aligning MBH MbhL, MBS MbsL, and complex I Nqo4, as in Figure 3, *C–F*. Notably, the C-terminal transmembranes immediately following loop 1 (highlighted in *semitransparent surface view*) are distinctively configured to coordinate the different numbers of the ion translocation units. *B*, the three-loop systems (marked by the *shaded area*) in complex I (*top*), MBH (*middle*), and MBS (*bottom*) are differently linked to membrane arm (semitransparent surface) through the variable C-terminal transmembranes following loop 1. However, a central charged axis from the proximal [4Fe–4S] through the membrane arms is maintained in each complex. *Red spheres* represent negatively charged residues and *blue spheres* positively charged residues. MBH, membrane-bound hydrogenase; MBS, membrane-bound sulfane sulfur reductase.

triggers conformational changes in three protein loops around the substrate pocket, which propagate along a central charge axis in the membrane arm to drive proton translocation (8–10, 66). This mechanism has gained strong support from recent biochemical and structural studies (17–19). Recent trapping of multiple states of complex I provide a glimpse of this complicated coupling mechanism: substrate reduction can initiate the reorganization of neighboring loops, which then induce conformational coupling (at the interface between the anchor for the peripheral arm and the proton translocation arm) and subsequent electrostatic coupling in a central hydrophilic axis across the membrane arm (14). A detailed structural comparison revealed that key elements implied in the coupling mechanism of complex I also exist in other members of complex I–like superfamily (Fig. 4).

First, loops 1 to 3—corresponding to the Nqo7, Nqo4, and Nqo8 loops in *T. thermophilus* complex I or the ND3, 49 kDa, and ND1 loops in *Bos taurus* complex I—near the proximal [4Fe–4S] cluster are structurally conserved among complex I, MBH, and MBS, although there is little sequence-level conservation (Fig. 4A). These loops were proposed to sense quinone reduction and induce the initial conformational change in complex I (14). Second, despite the distinct location of the membrane-anchored peripheral module between MBS/MBH and complex I (Fig. 1), all the C-terminal regions of their loop 1 function to maintain the interface between the membrane-anchored peripheral arm and the ion-translocation module. These are helix HL and TMH2–3 of Nqo7 in complex I; helix HL and TMH1–2 of MbhI in MBH; and helix HL and TMH15–16 of MbsH' in MBS (Fig. 4B). This dynamic interface was proposed for conformational coupling in complex I (14). Third, a prominent, central, charged axis extending from the membrane anchor to the H$^+$-translocating unit is maintained in MBH and MBS, as in complex I (Fig. 4B). This continuous hydrophilic axis within the membrane interior is key for electrostatic coupling in complex I (14). Thus, in spite of their distinct overall architectures, the presence of these equivalent coupling elements implicates that the coupling mechanism is probably conserved among the respiratory complexes.

Summary

The complex I–like family of respiratory complexes now includes complex I, NDH, MBH, and MBS, which are evolutionarily related to the Mrp H$^+$/Na$^+$ antiporter. The most recent structures of these complexes have enabled us to understand their evolutionary trajectory at the atomic level. Structural comparison of these respiratory machineries highlights their modular evolution and reinforces the idea that the membrane-anchored peripheral module, the H$^+$-translocation unit, and the Na$^+$-translocation unit are independently evolving building blocks that are assembled differently in these respiratory complexes (Figs. 1 and 2) (43). Accordingly, the structures reveal how the respiratory machinery has evolved to acquire unique redox capabilities by utilizing different redox substrates as they became available on the evolutionary time scale (Fig. 3).

Despite the different redox chemistries, the mechanism of energy conversion from redox potential to membrane proton gradient has been largely conserved across evolution (Fig. 4). The cryo-EM structures of the complex I–like superfamily provide us unprecedented knowledge into these complicated machineries. The determination of their ion translocation stoichiometry and molecular dynamics simulations based on these new structures will greatly help to understand their mechanisms. Solving the structures of substrate-bound or other coupling states will be required to answer important points such as the utilization of different substrates, ion translocation, and the coupling mechanism between them. Likewise, the differential arrangement of H$^+$ and Na$^+$ translocation modules in the currently available structures demonstrates that sequence homology is not sufficient to predict function, further demonstrating the need for the structures of additional complex I–related respiratory complexes.

Major questions on this intriguing group of respiratory complexes remain

- Are the charge core of the membrane domain and three-loop cluster the main elements responsible for energy transduction?
- Is the change of the NQ-P module angle in complex I, which might be part of the energy transduction process (14), a universal mechanism, and can it also be applied to MBH/MBS-type complexes?

Conflict of interest—The authors declare that they have no conflicts of interest with the contents of this article.

Abbreviations—The abbreviations used are: Fd, ferredoxin; MBH, membrane-bound hydrogenase; MBS, membrane-bound sulfane sulfur reductase; Mrp, multiple resistance and Ph; NDH, NADH dehydrogenase-like complex type-1; PQ, plastoquinone.

References

1. Sazanov, L. A. (2015) A giant molecular proton pump: Structure and mechanism of respiratory complex I. *Nat. Rev. Mol. Cell Biol.* **16**, 375–388
2. Hirst, J. (2013) Mitochondrial complex I. *Annu. Rev. Biochem.* **82**, 551–575

3. Schut, G. J., Zadvornyy, O., Wu, C. H., Peters, J. W., Boyd, E. S., and Adams, M. W. (2016) The role of geochemistry and energetics in the evolution of modern respiratory complexes from a proton-reducing ancestor. *Biochim. Biophys. Acta* **1857**, 958–970

4. Letts, J. A., and Sazanov, L. A. (2017) Clarifying the supercomplex: The higher-order organization of the mitochondrial electron transport chain. *Nat. Struct. Mol. Biol.* **24**, 800–808

5. Agip, A. A., Blaza, J. N., Fedor, J. G., and Hirst, J. (2019) Mammalian respiratory complex I through the lens of cryo-EM. *Annu. Rev. Biophys.* **48**, 165–184

6. Berrisford, J. M., Baradaran, R., and Sazanov, L. A. (2016) Structure of bacterial respiratory complex I. *Biochim. Biophys. Acta* **1857**, 892–901

7. Parey, K., Wirth, C., Vonck, J., and Zickermann, V. (2020) Respiratory complex I - structure, mechanism and evolution. *Curr. Opin. Struct. Biol.* **63**, 1–9

8. Galemou Yoga, E., Angerer, H., Parey, K., and Zickermann, V. (2020) Respiratory complex I - mechanistic insights and advances in structure determination. *Biochim. Biophys. Acta Bioenerg.* **1861**, 148153

9. Baradaran, R., Berrisford, J. M., Minhas, G. S., and Sazanov, L. A. (2013) Crystal structure of the entire respiratory complex I. *Nature* **494**, 443–448

10. Zickermann, V., Wirth, C., Nasiri, H., Siegmund, K., Schwalbe, H., Hunte, C., and Brandt, U. (2015) Structural biology. Mechanistic insight from the crystal structure of mitochondrial complex I. *Science* **347**, 44–49

11. Zhu, J., Vinothkumar, K. R., and Hirst, J. (2016) Structure of mammalian respiratory complex I. *Nature* **536**, 354–358

12. Fiedorczuk, K., Letts, J. A., Degliesposti, G., Kaszuba, K., Skehel, M., and Sazanov, L. A. (2016) Atomic structure of the entire mammalian mitochondrial complex I. *Nature* **538**, 406–410

13. Guo, R., Zong, S., Wu, M., Gu, J., and Yang, M. (2017) Architecture of human mitochondrial respiratory megacomplex I2III2IV2. *Cell* **170**, 1247–1257.e1212

14. Kampjut, D., and Sazanov, L. A. (2020) The coupling mechanism of mammalian respiratory complex I. *Science* **370**, eabc4209

15. Vinothkumar, K. R., Zhu, J., and Hirst, J. (2014) Architecture of mammalian respiratory complex I. *Nature* **515**, 80–84

16. Letts, J. A., Fiedorczuk, K., and Sazanov, L. A. (2016) The architecture of respiratory supercomplexes. *Nature* **537**, 644–648

17. Agip, A. A., Blaza, J. N., Bridges, H. R., Viscomi, C., Rawson, S., Muench, S. P., and Hirst, J. (2018) Cryo-EM structures of complex I from mouse heart mitochondria in two biochemically defined states. *Nat. Struct. Mol. Biol.* **25**, 548–556

18. Letts, J. A., Fiedorczuk, K., Degliesposti, G., Skehel, M., and Sazanov, L. A. (2019) Structures of respiratory supercomplex I+III2 reveal functional and conformational crosstalk. *Mol. Cell* **75**, 1131–1146.e1136

19. Cabrera-Orefice, A., Yoga, E. G., Wirth, C., Siegmund, K., Zwicker, K., Guerrero-Castillo, S., Zickermann, V., Hunte, C., and Brandt, U. (2018) Locking loop movement in the ubiquinone pocket of complex I disengages the proton pumps. *Nat. Commun.* **9**, 4500

20. Shikanai, T. (2016) Chloroplast NDH: A different enzyme with a structure similar to that of respiratory NADH dehydrogenase. *Biochim. Biophys. Acta* **1857**, 1015–1022

21. Peltier, G., Aro, E. M., and Shikanai, T. (2016) NDH-1 and NDH-2 plastoquinone reductases in oxygenic photosynthesis. *Annu. Rev. Plant Biol.* **67**, 55–80

22. Laughlin, T. G., Bayne, A. N., Trempe, J. F., Savage, D. F., and Davies, K. M. (2019) Structure of the complex I-like molecule NDH of oxygenic photosynthesis. *Nature* **566**, 411–414

23. Schuller, J. M., Birrell, J. A., Tanaka, H., Konuma, T., Wulfhorst, H., Cox, N., Schuller, S. K., Thiemann, J., Lubitz, W., Setif, P., Ikegami, T., Engel, B. D., Kurisu, G., and Nowaczyk, M. M. (2019) Structural adaptations of photosynthetic complex I enable ferredoxin-dependent electron transfer. *Science* **363**, 257–260

24. Pan, X., Cao, D., Xie, F., Xu, F., Su, X., Mi, H., Zhang, X., and Li, M. (2020) Structural basis for electron transport mechanism of complex I-like photosynthetic NAD(P)H dehydrogenase. *Nat. Commun.* **11**, 610

25. Sapra, R., Bagramyan, K., and Adams, M. W. (2003) A simple energy-conserving system: Proton reduction coupled to proton translocation. *Proc. Natl. Acad. Sci. U. S. A.* **100**, 7545–7550

26. Mayer, F., and Muller, V. (2014) Adaptations of anaerobic archaea to life under extreme energy limitation. *FEMS Microbiol. Rev.* **38**, 449–472

27. Kim, Y. J., Lee, H. S., Kim, E. S., Bae, S. S., Lim, J. K., Matsumi, R., Lebedinsky, A. V., Sokolova, T. G., Kozhevnikova, D. A., Cha, S. S., Kim, S. J., Kwon, K. K., Imanaka, T., Atomi, H., Bonch-Osmolovskaya, E. A., et al. (2010) Formate-driven growth coupled with H(2) production. *Nature* **467**, 352–355

28. Lim, J. K., Mayer, F., Kang, S. G., and Muller, V. (2014) Energy conservation by oxidation of formate to carbon dioxide and hydrogen via a sodium ion current in a hyperthermophilic archaeon. *Proc. Natl. Acad. Sci. U. S. A.* **111**, 11497–11502

29. Nisbet, E. G., and Sleep, N. H. (2001) The habitat and nature of early life. *Nature* **409**, 1083–1091

30. Kengen, S. W. M. (2017) 'Pyrococcus furiosus, 30 years on'. *Microb. Biotechnol.* **10**, 1441–1444

31. Wu, C. H., Schut, G. J., Poole, F. L., 2nd, Haja, D. K., and Adams, M. W. W. (2018) Characterization of membrane-bound sulfane reductase: A missing link in the evolution of modern day respiratory complexes. *J. Biol. Chem.* **293**, 16687–16696

32. McTernan, P. M., Chandrayan, S. K., Wu, C. H., Vaccaro, B. J., Lancaster, W. A., Yang, Q., Fu, D., Hura, G. L., Tainer, J. A., and Adams, M. W. (2014) Intact functional fourteen-subunit respiratory membrane-bound [NiFe]-hydrogenase complex of the hyperthermophilic archaeon Pyrococcus furiosus. *J. Biol. Chem.* **289**, 19364–19372

33. Schut, G. J., Lipscomb, G. L., Nguyen, D. M., Kelly, R. M., and Adams, M. W. (2016) Heterologous production of an energy-conserving carbon monoxide dehydrogenase complex in the hyperthermophile Pyrococcus furiosus. *Front. Microbiol.* **7**, 29

34. Pisa, K. Y., Huber, H., Thomm, M., and Muller, V. (2007) A sodium ion-dependent A1AO ATP synthase from the hyperthermophilic archaeon Pyrococcus furiosus. *FEBS J.* **274**, 3928–3938

35. Schut, G. J., Bridger, S. L., and Adams, M. W. (2007) Insights into the metabolism of elemental sulfur by the hyperthermophilic archaeon Pyrococcus furiosus: Characterization of a coenzyme A- dependent NAD(P)H sulfur oxidoreductase. *J. Bacteriol.* **189**, 4431–4441

36. Bridger, S. L., Clarkson, S. M., Stirrett, K., DeBarry, M. B., Lipscomb, G. L., Schut, G. J., Westpheling, J., Scott, R. A., and Adams, M. W. (2011) Deletion strains reveal metabolic roles for key elemental sulfur-responsive proteins in Pyrococcus furiosus. *J. Bacteriol.* **193**, 6498–6504

37. Schicho, R. N., Ma, K., Adams, M. W., and Kelly, R. M. (1993) Bioenergetics of sulfur reduction in the hyperthermophilic archaeon Pyrococcus furiosus. *J. Bacteriol.* **175**, 1823–1830

38. Jormakka, M., Yokoyama, K., Yano, T., Tamakoshi, M., Akimoto, S., Shimamura, T., Curmi, P., and Iwata, S. (2008) Molecular mechanism of energy conservation in polysulfide respiration. *Nat. Struct. Mol. Biol.* **15**, 730–737

39. Enemark, J. H., and Cosper, M. M. (2002) Molybdenum enzymes and sulfur metabolism. *Met. Ions Biol. Syst.* **39**, 621–654

40. Yu, H., Haja, D. K., Schut, G. J., Wu, C. H., Meng, X., Zhao, G., Li, H., and Adams, M. W. W. (2020) Structure of the respiratory MBS complex reveals iron-sulfur cluster catalyzed sulfane sulfur reduction in ancient life. *Nat. Commun.* **11**, 5953

41. Yu, H., Wu, C. H., Schut, G. J., Haja, D. K., Zhao, G., Peters, J. W., Adams, M. W. W., and Li, H. (2018) Structure of an ancient respiratory system. *Cell* **173**, 1636–1649.e1616

42. Schut, G. J., Boyd, E. S., Peters, J. W., and Adams, M. W. (2013) The modular respiratory complexes involved in hydrogen and sulfur metabolism by heterotrophic hyperthermophilic archaea and their evolutionary implications. *FEMS Microbiol. Rev.* **37**, 182–203

43. Efremov, R. G., and Sazanov, L. A. (2012) The coupling mechanism of respiratory complex I - a structural and evolutionary perspective. *Biochim. Biophys. Acta* **1817**, 1785–1795

44. Brandt, U. (2019) Adaptations of an ancient modular machine. *Science* **363**, 230–231

45. Hedderich, R. (2004) Energy-converting [NiFe] hydrogenases from archaea and extremophiles: Ancestors of complex I. *J. Bioenerg. Biomembr.* **36**, 65–75

46. Steiner, J., and Sazanov, L. (2020) Structure and mechanism of the Mrp complex, an ancient cation/proton antiporter. *Elife* **9**, e59407

47. Li, B., Zhang, K., Nie, Y., Wang, X., Zhao, Y., Zhang, X. C., and Wu, X. L. (2020) Structure of the Dietzia Mrp complex reveals molecular mechanism of this giant bacterial sodium proton pump. *Proc. Natl. Acad. Sci. U. S. A.* **117**, 31166–31176

48. Sazanov, L. A., and Hinchliffe, P. (2006) Structure of the hydrophilic domain of respiratory complex I from Thermus thermophilus. *Science* **311**, 1430–1436

49. Galkin, A. S., Grivennikova, V. G., and Vinogradov, A. D. (1999) −>H+/2e- stoichiometry in NADH-quinone reductase reactions catalyzed by bovine heart submitochondrial particles. *FEBS Lett.* **451**, 157–161

50. Wikstrom, M. (1984) Two protons are pumped from the mitochondrial matrix per electron transferred between NADH and ubiquinone. *FEBS Lett.* **169**, 300–304

51. Galkin, A., Drose, S., and Brandt, U. (2006) The proton pumping stoichiometry of purified mitochondrial complex I reconstituted into proteoliposomes. *Biochim. Biophys. Acta* **1757**, 1575–1581

52. Efremov, R. G., and Sazanov, L. A. (2011) Structure of the membrane domain of respiratory complex I. *Nature* **476**, 414–420

53. Kaila, V. R., Wikstrom, M., and Hummer, G. (2014) Electrostatics, hydration, and proton transfer dynamics in the membrane domain of respiratory complex I. *Proc. Natl. Acad. Sci. U. S. A.* **111**, 6988–6993

54. Di Luca, A., Gamiz-Hernandez, A. P., and Kaila, V. R. I. (2017) Symmetry-related proton transfer pathways in respiratory complex I. *Proc. Natl. Acad. Sci. U. S. A.* **114**, E6314–E6321

55. Kaila, V. R. I. (2018) Long-range proton-coupled electron transfer in biological energy conversion: Towards mechanistic understanding of respiratory complex I. *J. R. Soc. Interface* **15**, 20170916

56. Euro, L., Belevich, G., Verkhovsky, M. I., Wikstrom, M., and Verkhovskaya, M. (2008) Conserved lysine residues of the membrane subunit NuoM are involved in energy conversion by the proton-pumping NADH: ubiquinone oxidoreductase (complex I). *Biochim. Biophys. Acta* **1777**, 1166–1172

57. Zhu, S., and Vik, S. B. (2015) Constraining the lateral helix of respiratory complex I by cross-linking does not impair enzyme activity or proton translocation. *J. Biol. Chem.* **290**, 20761–20773

58. Belevich, G., Knuuti, J., Verkhovsky, M. I., Wikstrom, M., and Verkhovskaya, M. (2011) Probing the mechanistic role of the long alpha-helix in subunit L of respiratory complex I from Escherichia coli by site-directed mutagenesis. *Mol. Microbiol.* **82**, 1086–1095

59. Morino, M., Natsui, S., Ono, T., Swartz, T. H., Krulwich, T. A., and Ito, M. (2010) Single site mutations in the hetero-oligomeric Mrp antiporter from alkaliphilic Bacillus pseudofirmus OF4 that affect Na+/H+ antiport activity, sodium exclusion, individual Mrp protein levels, or Mrp complex formation. *J. Biol. Chem.* **285**, 30942–30950

60. Coincon, M., Uzdavinys, P., Nji, E., Dotson, D. L., Winkelmann, I., Abdul-Hussein, S., Cameron, A. D., Beckstein, O., and Drew, D. (2016) Crystal structures reveal the molecular basis of ion translocation in sodium/proton antiporters. *Nat. Struct. Mol. Biol.* **23**, 248–255

61. Lee, C., Kang, H. J., von Ballmoos, C., Newstead, S., Uzdavinys, P., Dotson, D. L., Iwata, S., Beckstein, O., Cameron, A. D., and Drew, D. (2013) A two-domain elevator mechanism for sodium/proton antiport. *Nature* **501**, 573–577

62. Wohlert, D., Kuhlbrandt, W., and Yildiz, O. (2014) Structure and substrate ion binding in the sodium/proton antiporter PaNhaP. *Elife* **3**, e03579

63. Hunte, C., Screpanti, E., Venturi, M., Rimon, A., Padan, E., and Michel, H. (2005) Structure of a Na+/H+ antiporter and insights into mechanism of action and regulation by pH. *Nature* **435**, 1197–1202

64. Page, C. C., Moser, C. C., Chen, X., and Dutton, P. L. (1999) Natural engineering principles of electron tunnelling in biological oxidation-reduction. *Nature* **402**, 47–52

65. Kashani-Poor, N., Zwicker, K., Kerscher, S., and Brandt, U. (2001) A central functional role for the 49-kDa subunit within the catalytic core of mitochondrial complex I. *J. Biol. Chem.* **276**, 24082–24087

66. Parey, K., Brandt, U., Xie, H., Mills, D. J., Siegmund, K., Vonck, J., Kuhlbrandt, W., and Zickermann, V. (2018) Cryo-EM structure of respiratory complex I at work. *Elife* **7**, e39213